

Short Communication

A Novel Synthesis of triangular Pt Nanosheets on Pd surface with a Strong Electrocatalytic Activity for Oxidation of Methanol

Tran Thi Bich Quyen^{1,*}, Nguyen Phu Qui¹, Vo Le Nhat An¹, Nguyen Thi Tho²,
Luong Huynh Vu Thanh¹, Bui Le Anh Tuan³, Tan-Thanh Huynh⁴

¹ Department of Chemical Engineering, College of Engineering Technology, Can Tho University, 3/2 Street, Ninh Kieu District, Can Tho City, Vietnam

² Institute of Applied Science, Ho Chi Minh City University of Technology, 475B Dien Bien Phu Street, Ward 25, Binh Thanh District, HCM city, Vietnam

³ Department of Civil, College of Technology, Can Tho University, 3/2 Street, Ninh Kieu District, Can Tho City, Vietnam

⁴ Tra Vinh University, 126 Nguyen Thien Thanh, Ward 4, District 5, Tra Vinh City, Vietnam

*E-mail: ttbquyen@ctu.edu.vn

Received: 29 January 2019 / Accepted: 19 March 2019 / Published: 30 June 2019

The study presents three-dimensional Pd/Pt triangular nanosheets with controlled shape and composition synthesized by a novel approach that uses lemon extract as a biological reducing agent coupled with a microwave treatment at 80 W (~64°C) for 30 min, which proved to be a simple, rapid, and environmentally-friendly method. The morphology, structure, and composition of prepared Pd/Pt triangular nanosheets were identified by transmission electronic microscopy (TEM), X-ray diffraction (XRD), and energy-dispersive X-ray (EDX) techniques. Moreover, the electrocatalytic properties of these synthesized Pd/Pt triangular nanosheets (Pd/Pt TANSs), and Pd@Au core/shell nanosheet (Pd@Au NS), and Pd nanosheet (Pd NS) electrocatalysts for methanol oxidation reaction (MOR) were systematically researched using the cyclic voltammetry method. The results showed that Pd/Pt triangular nanosheet (Pd/Pt TANS) electrocatalysts provided a stronger catalytic activity of about ~2.4 and ~1.4 times that of Pd NS and Pt@Au NS catalysts for MOR. In addition, these new triangular nanosheet electrocatalysts achieved a higher MOR performance with decreased use of Pt. This method can create a general approach for the shape-controlled synthesis of bimetallic Pt/M (M = Pd, Cu, Au, Mo, Mn, etc.) triangular nanocatalysts for promising applications in fuel cells in the future.

Keywords: Pd/Pt triangular nanosheets (Pd/Pt TANSs); novel synthesis; catalytic activity; methanol oxidation reaction (MOR); Pt nanotriangles (Pt NTAs).

1. INTRODUCTION

For many years, advances in nanotechnology and metal nanocrystals have caught the attention of scientists and industrial producers owing to their ordinary applications in plasmonics, magnetic materials, catalysis, electronic devices, and biomedicine (i.e., drug delivery, and cancer diagnosis for example) [1–16]. In addition, nanomaterials have proved to have typical properties that are greater than those of bulk materials [17–24]. Therefore, modifying their plasmonic properties and catalytic activity plays a very important role in the advances in many fields such as catalysis, surface-enhanced Raman scattering, energy harvesting and conversion, sensing, photovoltaic devices, photocatalysis and imaging [16, 25–29].

Structural modification of noble metal nanostructures at the atomic scale can highly increase their optical and catalytic properties [30–32]. Thus, ornamenting the surface of single-crystal metal substrates using single-layer or few-layer graphene generates the lattice strain, which has a key role in determining the surface reactivity [33, 34]. Furthermore, bimetallic core/shell or dendrite nanostructures with an atomically thin shell or small particle sizes have been synthesized and used to improve the catalytic activities [35–40].

Palladium (Pd) is a key component of many catalysts used in industrial processes and commercial devices [41]. Pd is a flexible catalyst for a large number of significant industrial reactions such as the important C-C coupling reactions and hydrogenation of unsaturated organic compounds [42–48]. Moreover, Pd is a good material for hydrogen storage and sensing [49, 50]. For instance, Pd nanowire arrays, Pd/Pt nanoalloys and Pd-Cu nanoalloy thin film were discovered to be very active catalysts for ethanol oxidation in direct alcohol fuel cells, for methanol oxidation reactions and as catalysts for Suzuki-Miyaura or Sonogashira coupling reactions [51–54]. Accordingly, controlling the shape of Pd nanostructures was crucial in increasing their catalytic activities as well as in applying their properties for many applications such as SERS and optical sensing [55–57]. Further, it has been previously reported that two-dimensional Pd nanoparticles display ferromagnetic characteristics that differ from those of bulk Pd [58–60]. Additionally, recent research also showed that the Pd nanoplates have a greater capacity for hydrogen absorption than that of bulk Pd and spherical Pd nanoparticles [53, 61–63].

To the best of our knowledge, the synthesis of Pd/Pt triangular nanosheets has not been reported previously. Pt has a high cost, sluggish kinetics and poor durability of Pt catalysts, which have limited its wide spread commercialization of fuel cells [64]. Using Pt-based dendritic nanosheets as new catalysts may solve these above problems and allow for more commercial opportunities in fuel cells because of the following advantages: 1) Applying the nanosheets helps reduce the used concentration of Pt based on dendrite nanostructures consisting of Pt nanoparticles on appropriate monometallics; 2) The nanosheets have high surface-to-volume ratios and terrace sites – the active sites for the methanol oxidation reaction (MOR) and to enhance the redox reactions due to their high catalytic activity and stability [24, 40, 65–67]; 3) The nanosheets also dramatically diminish the dissolution of Pt due to their low number of edges and corners with low coordinate sites [68].

As a result, this study has been carried out for a rapid, simple, green and beneficial approach to synthesize ultrathin Pd nanosheets with Pt nano-triangular particles on their surface by using lemon extract as a biological reducing agent coupled with microwave treatment. We developed a synthetic

method with a quick reaction time, that was cost effective, easy to perform, and resulted in uniform particle sizes with stable and sustainable properties. Additionally, the synthesized Pd/Pt triangular nanosheets show promising applications as good catalysts (i.e., fuel cells, and sensing, etc.) both now and in the future.

2. EXPERIMENTAL SECTION

2.1 Materials

Palladium (II) acetylacetonate ($\text{Pd}(\text{acac})_2$, 99%), polyvinylpyrrolidone (PVP; $M_{\text{wt}} \sim 10,000$), tungsten hexacarbonyl ($\text{W}(\text{CO})_6$; 97%), hexachloroplatinic acid hexahydrate ($\text{H}_2\text{PtCl}_6 \cdot 6\text{H}_2\text{O}$, 50% Pt basis), rhodamine 6G (R6G; $\geq 99\%$), and N,N-Dimethylformamide (DMF) were purchased from Sigma-Aldrich and Merck. Cetyltrimethylammonium bromide (CTAB), ascorbic acid (AA), acetone, methanol and ethanol were purchased from Acros. Fresh lemons (~3 months old, green shell) were bought from a garden in Phong Dien, Can Tho City in Vietnam. All solutions were prepared with deionized water from a MilliQ system.

2.2 Methods

2.2.1. Preparation of lemon extract

Fresh lemons were squeezed for juice. The lemon juice was then filtered, centrifuged and washed with deionized (DI) water three times to obtain an extract. This lemon extract was used for the synthesis of Pd/Pt triangular nanosheets (Pd NSs) in the following steps.

2.2.2 Preparation of Pd nanosheets

Palladium nanosheets (Pd NSs) were synthesized by a simple and effective approach using tungsten hexacarbonyl ($\text{W}(\text{CO})_6$) as a reducing agent without CO gas. In a typical synthesis, 60 mg of CTAB and 30 mg of PVP were dissolved in 10 mL of DMF, then 16 mg of $\text{Pd}(\text{acac})_2$ and 1 mL of lemon extract were added and stirred for 20 min at room temperature. The stirred homogeneous solution was transferred into a 50 ml flask and 100 mg of $\text{W}(\text{CO})_6$ was quickly poured into the flask as a reducing agent for the reduction of $\text{Pd}(\text{acac})_2$. Finally, the solution was continuously stirred and heated at 90°C for 90 minutes, then centrifuged (12000 rpm; 15 min) and washed with acetone/ethanol to remove excess and redispersed in ethanol/deionized water (DI H_2O). The average size of the prepared Pd nanosheets is approximately 20–30 nm.

2.2.2 Synthesis of Pd/Pt triangular nanosheets

In a particular synthesis of Pd/Pt triangular nanosheets, 100 μL of lemon extract was poured dropwise into 10 mL of the synthesized mixture of Pd nanosheet solution before being centrifuged and

various volumes of the 1 mM platinum salt ($\text{H}_2\text{PtCl}_6 \cdot 6\text{H}_2\text{O}$) solution of 300 μL ; 400 μL ; 500 μL and 1 mL were also added dropwise into the centrifuged solution and stirred for 10 min at room temperature. Next, the stirred solution was heated by a microwave at 80 W ($\sim 64^\circ\text{C}$) for 30 min. Later, the heated solution was centrifuged again, washed several times with acetone/deionized water to remove excess and redispersed in deionized water (DI H_2O) to obtain the Pd/Pt triangular nanosheets (Pd/Pt TANSs) with the average size of the prepared Pd nanosheets (Pd NSs) being 20–30 nm and the of Pt nanotriangles (Pt NTAs) of ~ 5 –7.5 nm deposited uniformly on the Pd nanosheet's surfaces.

2.2.4 Characterization techniques and CV measurements

The absorbance spectra of the solutions of Pd/Pt triangular nanosheets were determined by UV–vis spectrophotometry (UV-675; Shimadzu). The phase structure of the Pd/Pt triangular nanosheets was examined using an X-ray diffractometer (Rigaku Dmax-B, Japan) with $\text{Cu K}\alpha$ source operated at 40 kV and 100 mA. A scan rate of 0.05 deg^{-1} was used for 2θ between 30° and 90° . The shape, particle size, and elemental analysis by Energy-dispersive X-ray spectroscopy (EDX or EDS) of Pd/Pt triangular nanosheets were examined by transmission electron microscope (TEM) with a Philips Tecnai F20 G2 FEI-TEM microscope (accelerating voltage 200 kV).

2.2.5 Electrode preparation and electrochemical measurements of Pd/Pt triangular nanosheets

A three-electrode cell connected to a Solartron 1480 potentiostat/galvanostat was used for electrochemical measurements. A high surface area Pt and a saturated calomel electrode were used as counter and reference electrodes, respectively. All potentials in this work are referred to Ag/AgCl reference electrode. A thin layer of a Nafion-impregnated catalyst cast on a glassy carbon (GC) disc (PINE) of 5 mm diameter (0.1964 cm^2 area) embedded in a Teflon holder was used for the working electrode. A determined amount of the catalyst was dispersed in 0.5% Nafion by sonication for 15 min, and 7 μL of the Pd/Pt triangular nanosheet catalyst suspension containing $0.112 \text{ mg Pt mL}^{-1}$ was placed on a glassy carbon electrode (GCE) surface and dried at 80°C for 10 min to yield a uniform thin film. Prior to catalyst coating, the GCE surface was polished with $0.3 \mu\text{m}$ alumina powder (BAS), cleaned with ethanol and washed with copious amounts of deionized water (Procedure 1).

An aqueous solution of H_2SO_4 of 0.5 M was used as an electrolyte in all electrochemical measurements. In cyclic voltammetry (CV), the potential was swept between -0.2 and 1.0 V at a scan rate (ν) of 50 mV s^{-1} .

A solution of 10 % v/v CH_3OH in the aqueous H_2SO_4 of 0.5 M was used as the electrolyte for all the methanol oxidation reaction (MOR) studies. In CV, the potential was swept between 0.0 and 1.2 V at a scan rate (ν) of 50 mV s^{-1} . Before the CV measurements were carried out, the electrode was activated in the same solution by potential cycling of 30 times in the range of 0.0 to 1.2 V at $\nu = 50 \text{ mV s}^{-1}$. Steady-state polarization measurements of MOR were conducted from 0.0 to 1.2 V at $\nu = 50 \text{ mV s}^{-1}$ with the electrode rotated at 1600 rpm. In all above methanol oxidation studies, the electrolyte was deaerated with Ar gas for 30 min before measurements, and the gas was passed above the solution level during the

experiments. All electrochemical experiments were carried out at $(25\pm 1)^{\circ}\text{C}$. Working electrodes of Nafion-impregnated catalyst Pd nanosheets (Pd NSs), Pd@Au core/shell nanosheets (Pd@Au NSs), and Pd/Pt triangular nanosheets (Pd/Pt TNSs) on GCEs were prepared by the same procedure as above (Procedure 1) for electrochemical measurements. Pt loading was maintained at 0.112 mg cm^{-2} on all the catalyst electrodes in the electrochemical studies.

3. RESULTS AND DISCUSSION

3.1 Characterization and morphology of the Pd/Pt triangular nanosheets

As shown in Figure 1, the UV-vis spectra of the Pd/Pt triangular nanosheets (Pd/Pt TANSs) exhibit a maximum absorbance in the range of 967 nm to 1005 nm. The maximum absorbance of the Pd/Pt TANS samples is at 986 nm and indexed into the NIR region shown in Figure 1(c).

In addition, increasing the reaction time leads to enhancing the value of maximum absorbance and shifts to the near-infrared region (NIR) at 986 nm instead of 967 nm as presented in Figure 1(a–c). However, the reaction time is significantly increased at 45 min, leading to the maximum absorbance gradually decreasing – as shown in Figure 1(d). Therefore, the optimal sample with the reaction time of 30 min in the microwave will be chosen to investigate other factors in the next steps for the synthesis of Pd/Pt triangular nanosheets (Pd/Pt TANSs).

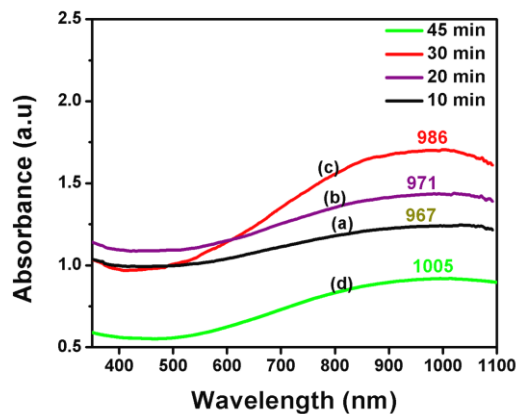


Figure 1. UV-vis spectra of Pd/Pt triangular nanosheets (Pd/Pt TANSs) with a microwave treatment of 80 W ($\sim 64^{\circ}\text{C}$) for various reaction times of: (a) 10 min; (b) 20 min; (c) 30 min; and (d) 45 min.

This finding was supported by the transmission electron microscopy (TEM) image of the Pd/Pt triangular nanosheets (Pd/Pt TANSs). As shown in Figure 2, the representative TEM images of Pd/Pt triangular nanosheet (Pd/Pt TANS) samples and the Pd nanosheets still adopt a hexagonal plate-like shape and have an average diameter of $\sim 20\text{--}30\text{ nm}$ and the Pt nanotriangles with like-triangle shape (Pt NTAs) of $\sim 5\text{--}7.5\text{ nm}$. It demonstrated that the Pd/Pt triangular nanosheets (Pd/Pt TANSs) were respectively obtained with their nanostructure of the composite, non-structural of the core/shell or the alloy.

The study of the elemental distribution of Pt triangles on the Pd nanosheet surface was also performed using energy-dispersive X-ray spectroscopy (EDX). The results showed a distribution of 81.2% of Pd and 5.6% of Pt - see Figure 3. It indicated that Pt nanotriangles were successfully deposited and homogeneously diffused in the Pd nanosheet mixture.

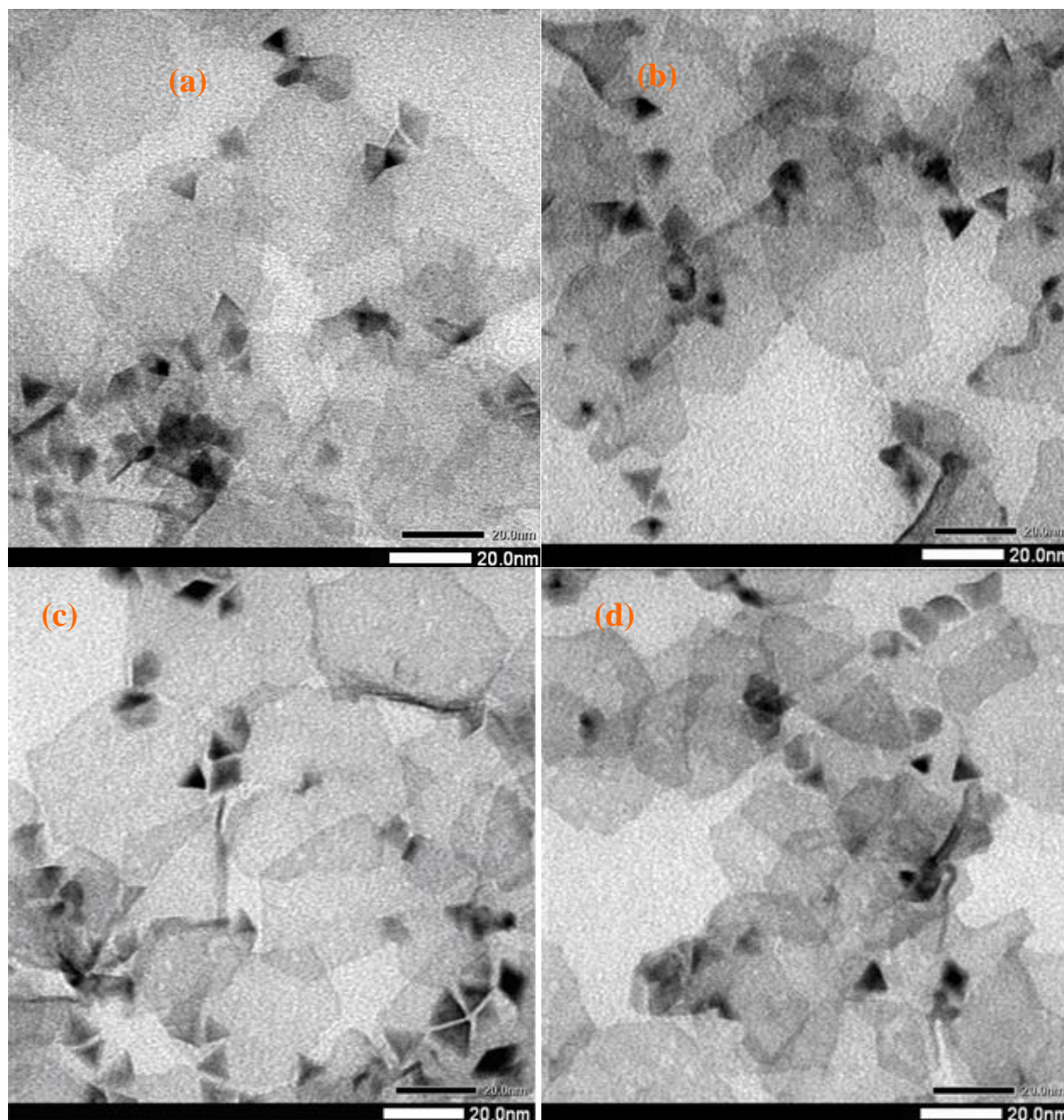


Figure 2. TEM images of Pd/Pt triangular nanosheets (Pd/Pt TANSs) with a microwave treatment of 80 W ($\sim 64^{\circ}\text{C}$) for various reaction times of (a) 10 min; (b) 20 min; (c) 30 min; and (d) 45 min.

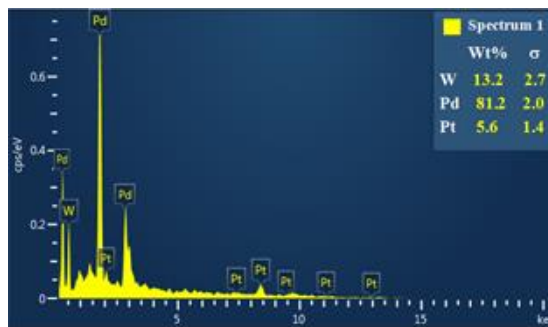


Figure 3. EDS profile of Pd/Pt triangular nanosheets and their quantitative analysis.

The structure of the Pd/Pt triangular nanosheets (Pd/Pt TANSs) was verified by X-ray diffraction (XRD). The PDF standard card was used to index these XRDs. As shown in Figure 4, the XRD peaks of the synthesized Pd/Pt triangular nanosheets (Pd/Pt TANSs), pure Pd and Pt nanocrystals could be indexed as a face-centered cubic (fcc) structure. The characteristic peaks of Pd achieved at 40.9° , 46.8° , 68.4° , 82.1° , 86.7° ; and of Pt at 40.2° , 46.1° , 65.7° , 78.7° , and 85.4° correspond to crystal facets of {111}, {200}, {220}, {311} and {222} of Pd and Pt as compared to and interpreted with standard data respective of pure fcc Pd (JCPDS No. 05-0681) and pure fcc Pt (JCPDS No. 87-0647), which proposed the successful synthesis of Pd/Pt triangular nanosheets (Pd/Pt TANSs) with composite nanostructures.

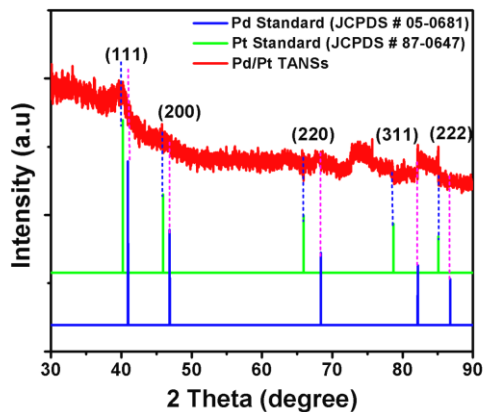


Figure 4. XRD pattern of Pd/Pt triangular nanosheets (Pd/Pt TANSs) (where the Pd/Pt TANSs were prepared as a thin film deposited on a silicon wafer).

3.2 Catalytic activity measurement of the Pd/Pt triangular nanosheets for methanol oxidation

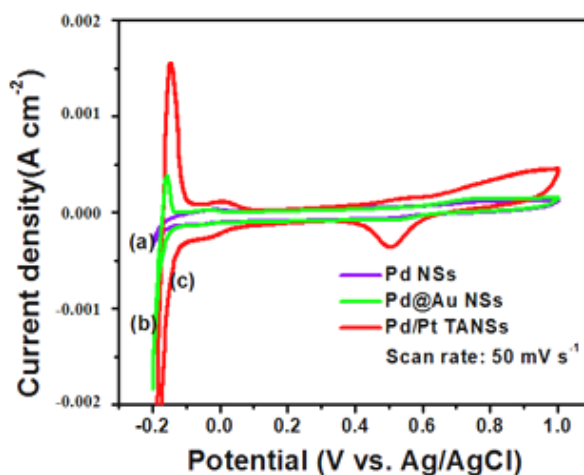


Figure 5. Cyclic voltammograms for (a) Pd nanosheets (Pd NSs), (b) Pd@Au core/shell nanosheets (Pd@Au NSs), and (c) Pd/Pt triangular nanosheets (Pd/Pt TANSs) in Ar-saturated 0.5 M H₂SO₄ solution at 25°C. Sweep rate = 50 mV s⁻¹. Pt loading of electrodes = 0.112 mg cm⁻².

The cyclic voltammetry (CV) curves of three catalysts (Pd/Pt TANSs, Pd NSs and Pd@Au NSs) were recorded at room temperature in Ar-purged 0.5 M H₂SO₄ solutions at a scan rate of 50 mV s⁻¹. The results noted that the peak current densities at a scan rate of 50 mV s⁻¹ were 376, 26, and 90 mA cm⁻², respectively showing that the activity of the Pd/Pt TANS catalyst (Pt loading of electrode = 0.112 mg cm⁻²) was ~15 times higher than that of the Pd NS catalyst and ~4 times stronger than that of the Pd@Au NS catalyst with the same Pd loading.

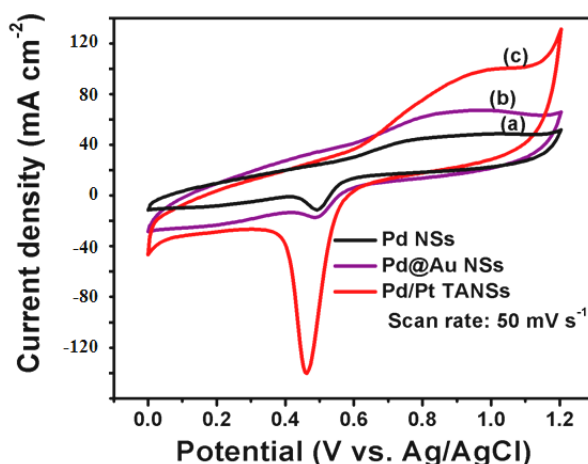


Figure 6. Cyclic voltammograms for methanol oxidation of (a) Pd nanosheets (Pd NSs), (b) Pd@Au core/shell nanosheets (Pd@Au NSs), and (c) Pd/Pt triangular nanosheets (Pd/Pt TANSs) in Ar-saturated 10 v/v% CH₃OH in 0.5 M H₂SO₄ solution at 25°C. Sweep rate = 50 mV s⁻¹. Pt loading of electrodes = 0.112 mg cm⁻².

The electrocatalytic properties of the Pd/Pt TANSs for the anodic MOR were evaluated. Two references Pt-based catalysts, Pd nanosheets (Pd NSs) and Pd@Au core/shell nanosheets (Pd@Au NSs) were also performed for comparison. As presented in Figure 6, the Pd/Pt TANS catalyst electrode showed a stronger electrocatalytic activity for methanol oxidation compared with that of Pd NS or Pd@Au NS catalyst electrodes. The results demonstrated (1) the lowest potential at the start time of methanol oxidation (onset potential, E_{onset}), (2) the highest methanol oxidation peak current (i_f), which indicates the extent of methanol oxidation capability, and (3) the highest ratio of i_f/i_b showing the electrode's efficiency in destroying CO-like residues. In addition, the onset potential of methanol oxidation was 572 mV, 655 mV, and 626 mV versus normal Ag/AgCl electrode for Pd/Pt TANSs, Pd NSs, and Pd@Au NSs, respectively.

The comparison of the catalytic activities of Pd/Pt TANSs, Pd NSs and Pd@Au NSs was also analyzed by linear sweep voltammetry (LSV), scanning from 0.0 to 1.2 V vs. Ag/AgCl with a scan rate of 50 mV s^{-1} at 1600 rpm – as shown in Figure 7. Noticeably, Pd/Pt TANSs helped the methanol oxidation occur at less positive potentials (572 mV) compared with Pd NSs (655 mV) and Pd@Au NSs (626 mV). The polarization currents were significantly larger for the Pd/Pt catalytic electrode in the entire potential region. For example, at 850 mV, the current density for the Pd/Pt TANSs was 1.4, and 2.4 times greater than for the Pd@Au NSs and Pd NSs, respectively. These results indicated that the Pd/Pt TANS catalyst exhibits higher electrocatalytic activity for methanol oxidation than that of Pd@Au NS and Pd NS catalysts.

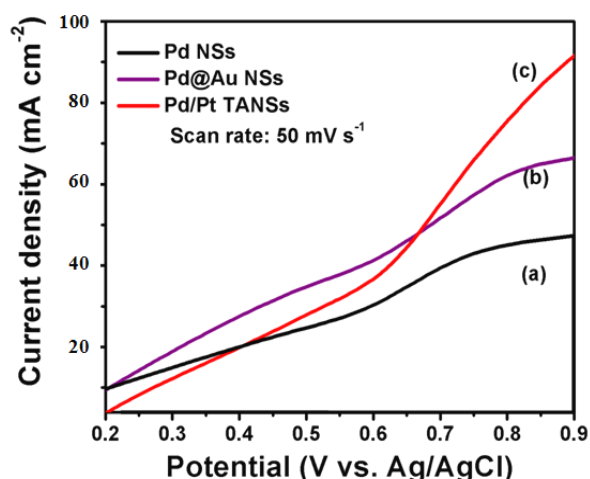


Figure 7. Steady-state anodic polarization curves for (a) Pd NSs, (b) Pd@Au NSs, and (c) Pd/Pt TANSs catalysts, sweep rate = 50 mV s^{-1} in Ar-saturated 10 v/v% CH_3OH in 0.5 M H_2SO_4 solution at 25°C . Electrode rotation speed = 1600 rpm. Pd loading electrode = 0.112 mg cm^{-2} .

The apparent activation energy of all synthesized electrocatalysts is shown in Table 1. The apparent activation energy was lower than those found for the Pd/Pt TANS electrode. This result indicated that Pt nanotriangles improved the electro-oxidation of methanol in the MOR process. The effects attributed to Pd/Pt TANSs are related to their high surface area, high electrical conductivity, upgraded electronic transference and the obtaining of more small and stable bimetallic nanoparticles.

Some of the values reported in the literature are compared with our data in Table 1. According to Table 1, most of the presence of Pd and Pt alloys or composites are better electrocatalysts for methanol oxidation than bulk materials. The catalytic activity can be influenced by the morphological, surface area, concentration and size effects. Thus, nanostructures with a high surface to volume ratio such as nanosheets with a high surface area can be good candidates in the field of electrocatalysis for MOR.

Table 1. Comparing different electrocatalysts for methanol oxidation reaction

Electrode	Onset Potential (V vs. RHE)	Anodic Peak Potential (V vs. NHE)	Anodic Peak Potential (V vs. RHE)	Anodic Peak Current (mA cm ⁻²)	Pt loading (mg cm ⁻²)	Reference
Au@Pd/RGO	0.500	-	-	28	-	[69]
Pd/RGO	0.700	-	-	4	-	[69]
Pd-NiO(2:1)/C	0.535	-	-	63	-	[70]
Pt/C	0.525	-	-	18	-	[70]
Pd/C	0.611	-	1.006	1.41	-	[71]
Pt/C	0.441	-	1.006	1.48	-	[71]
Pd-Ni(1:1)/C	-	-	0.914	7.64	-	[72]
Pd-Ag(2:1)/C	0.446	-	0.886	0.635	-	[73]
Pd-Ag(1:1)/C	0.436	-	0.856	0.678	-	[73]
Pt thin film	-	0.73	-	31.3	1	[74]
PtCo thin film	-	0.6	-	217.6	1	[52]
PdCu/RGO thin film	-	0.8	-	249.53	1	[52]
PtPdCu/RGO thin film	-	0.7	-	296.26	1	[52]
Pd NSs	0.655	-	0.85	47	-	This work
Pd@Au NSs	0.626	-	0.85	63	-	This work
Pd/Pt TANSs	0.572	-	0.85	88	0.112	This work

Generally, Pd-based catalysts or Pd-M alloys (M = Ag, Ni, Rh, Au, Cu, and Pt) have displayed various activities towards the methanol oxidation. In this work, Pt nanotriangles on Pd nanosheets induced a decrease in the methanol oxidation onset potential (0.572 V vs. RHE), in comparison with that observed for Pd NSs, Pd@Au NSs catalysts or Pd/C catalyst (0.611 V vs. RHE) [71], Pd/RGO catalyst (0.7 V vs. RHE) [69]. The addition of Pt promoted the easy removal of CO adsorption, increasing the number of active sites able to adsorb and oxidize methanol. The causes associated with the activity enhancement by Pt presence in the composite or alloy were explained from a displacement in the d-band center of Pd, affecting the electronic properties of this metal and the activation of water at lower potentials in comparison with those required for Pd, which participates in the oxidation of CO adsorption. Moreover, most of these Pd nanosheets are better electrocatalysts for methanol oxidation than bulk materials and also Pt nanotriangles that is due to the high specific surface area and high active sites that is due to the nanosheets structures of Pd. It is obvious that all the electronic, synergistic, geometric and morphological, stabilizer, surface area and size effects can influence the catalytic activity of the electrocatalysts. Thus, nanosheets with high surface area can be a good candidate in the field of electrocatalysis for methanol oxidation reaction (MOR). In addition, using non-noble metal near the Pd

or Pt can disturb the electronic structure of the Pt and Pd and change the highest occupied and lowest unoccupied molecular orbitals of these metals due to the electron transfer effect. The difference between the electronegativity of two atoms is the fact that causes electron density between atoms and leads to electron transfer.

4. CONCLUSIONS

In this study we have reported a simple, novel and rapid approach for the synthesis of Pd/Pt triangular nanosheets (Pd/Pt TANSs) using lemon extract as a biological reducing agent coupled with microwave treatment. The results demonstrated their very high activity and durability for methanol oxidation reactions (MORs) compared with those of Pd nanosheet (Pd NS) and Pd@Au core/shell nanosheet (Pd@Au NS) catalysts. Pd/Pt triangular nanosheets (Pd/Pt TANSs) have been applied as a new functional co-catalytic support for the MOR in fuel cell applications. The significant enhancement of catalytic activity and durability by the strong metal-metal interaction (nanocomposites), and co-catalytic and ultrahigh stability as well as the large surface area, provide more commercial opportunities for their applications in the MOR in fuel cells in comparison to Pd NSs and Pd@Au NSs catalysts. In fact, these findings provide a broad applicability of multifunctional Pd/Pt triangular nanosheets (Pd/Pt TANSs) in fuel cells and in other fields such as catalytic biosensor technology, and as electrochemistry sensors and catalysts.

ACKNOWLEDGEMENT

This research is funded by Vietnam National Foundation for Science and Technology Development (NAFOSTED) under grant number 103.99-2016.04.

References

1. C. N. R. M. Rao, A.; Cheetham, A. K, Eds., *Wiley-VCH Verlag GmbH & Co. KGaA: Weinheim*, (2004).
2. X. Huang, Z. Zeng and H. Zhang, *Chem. Soc. Rev.*, 42 (2013) 1934.
3. H. Zhang, *ACS Nano*, 9 (2015) 9451.
4. Q. Wang and D. O'Hare, *Chem. Rev.*, 112 (2012) 4124.
5. H. Liu, Y. Du, Y. Deng and P. D. Ye, *Chem. Soc. Rev.*, 44 (2015) 2732.
6. L. Dou, A. B. Wong, Y. Yu, M. Lai, N. Kornienko, S. W. Eaton, A. Fu, C. G. Bischak, J. Ma, T. Ding, N. S. Ginsberg, L.-W. Wang, A. P. Alivisatos and P. Yang, *Science*, 349 (2015) 1518.
7. Y. Peng, Y. Li, Y. Ban, H. Jin, W. Jiao, X. Liu and W. Yang, *Science*, 346 (2014) 1356.
8. C. Wang, H. Daimon, Y. Lee, J. Kim and S. Sun, *J. Am. Chem. Soc.*, 129 (2007) 6974.
9. S. Gao, Y. Lin, X. Jiao, Y. Sun, Q. Luo, W. Zhang, D. Li, J. Yang and Y. Xie, *Nature*, 529 (2016) 68.
10. S. Sun, C. B. Murray, D. Weller, L. Folks and A. Moser, *Science*, 287 (2000) 1989.
11. A. Hatzor and P. S. Weiss, *Science*, 291 (2001) 1019.
12. A. Eychmüller, *J. Phys. Chem. B*, 104 (2000) 6514.
13. M. A. El-Sayed, *Acc. Chem. Res.*, 34 (2001) 257.
14. W. U. Huynh, J. J. Dittmer and A. P. Alivisatos, *Science*, 295 (2002) 2425.

15. D. Jariwala, V. K. Sangwan, L. J. Lauhon, T. J. Marks and M. C. Hersam, *Chem. Soc. Rev.*, 42 (2013) 2824.
16. D. Jariwala, V. K. Sangwan, L. J. Lauhon, T. J. Marks and M. C. Hersam, *ACS Nano*, 8 (2014) 1102.
17. Z. Sun, T. Liao, Y. Dou, S. M. Hwang, M.-S. Park, L. Jiang, J. H. Kim and S. X. Dou, *Nat. Commun.*, 5 (2014) 3813.
18. T. T. B. Quyen, C.-C. Chang, W.-N. Su, Y.-H. Uen, C.-J. Pan, J.-Y. Liu, J. Rick, K.-Y. Lin and B.-J. Hwang, *J. Mater. Chem. B*, 2 (2014) 629.
19. A. Fukuoka, N. Higashimoto, Y. Sakamoto, S. Inagaki, Y. Fukushima and M. Ichikawa, *Micropor. Mesopor. Mater.*, 48 (2001) 171.
20. J. N. Kuhn, W. Huang, C.-K. Tsung, Y. Zhang and G. A. Somorjai, *J. Am. Chem. Soc.*, 130 (2008) 14026.
21. T. T. B. Quyen, W.-N. Su, K.-J. Chen, C.-J. Pan, J. Rick, C.-C. Chang and B.-J. Hwang, *J. Raman Spectrosc.*, 44 (2013) 1671.
22. X. Huang, S. Tang, X. Mu, Y. Dai, G. Chen, Z. Zhou, F. Ruan, Z. Yang and N. Zheng, *Nat. Nano*, 6 (2011) 28.
23. X. Huang, S. Li, Y. Huang, S. Wu, X. Zhou, S. Li, C. L. Gan, F. Boey, C. A. Mirkin and H. Zhang, *Nat. Commun.*, 2 (2011) 292.
24. F. J. Perez-Alonso, D. N. McCarthy, A. Nierhoff, P. Hernandez-Fernandez, C. Strebel, I. E. L. Stephens, J. H. Nielsen and I. Chorkendorff, *Angew. Chem. Int. Ed.*, 51 (2012) 4641.
25. F. Saleem, Z. Zhang, B. Xu, X. Xu, P. He and X. Wang, *J. Am. Chem. Soc.*, 135 (2013) 18304.
26. H. Duan, N. Yan, R. Yu, C.-R. Chang, G. Zhou, H.-S. Hu, H. Rong, Z. Niu, J. Mao, H. Asakura, T. Tanaka, P. J. Dyson, J. Li and Y. Li, *Nat. Commun.*, 5 (2014) 3093.
27. X. Yin, X. Liu, Y.-T. Pan, K. A. Walsh and H. Yang, *Nano Lett.*, 14 (2014) 7188.
28. J. W. Hong, Y. Kim, D. H. Wi, S. Lee, S.-U. Lee, Y. W. Lee, S.-I. Choi and S. W. Han, *Angew. Chem. Int. Ed.*, 55 (2016) 2753.
29. X. Wang, M. Vara, M. Luo, H. Huang, A. Ruditskiy, J. Park, S. Bao, J. Liu, J. Howe, M. Chi, Z. Xie and Y. Xia, *J. Am. Chem. Soc.*, 137 (2015) 15036.
30. L. Zhang, L. T. Roling, X. Wang, M. Vara, M. Chi, J. Liu, S.-I. Choi, J. Park, J. A. Herron, Z. Xie, M. Mavrikakis and Y. Xia, *Science*, 349 (2015) 412.
31. T. T. Bich Quyen, W.-N. Su, C.-H. Chen, J. Rick, J.-Y. Liu and B.-J. Hwang, *J. Mater. Chem. B*, 2 (2014) 5550.
32. T. T. B. Quyen and B.-J. Hwang, *Procedia CIRP*, 40 (2016) 551.
33. J. Zhang, M. B. Vukmirovic, Y. Xu, M. Mavrikakis and R. R. Adzic, *Angew. Chem. Int. Ed.*, 44 (2005) 2132.
34. J. Zhang, M. B. Vukmirovic, K. Sasaki, A. U. Nilekar, M. Mavrikakis and R. R. Adzic, *J. Am. Chem. Soc.*, 127 (2005) 12480.
35. V. T. T. Ho, C.-J. Pan, J. Rick, W.-N. Su and B.-J. Hwang, *J. Am. Chem. Soc.*, 133 (2011) 11716.
36. M. Shao, K. Shoemaker, A. Peles, K. Kaneko and L. Protsailo, *J. Am. Chem. Soc.*, 132 (2010) 9253.
37. K. Gong, D. Su and R. R. Adzic, *J. Am. Chem. Soc.*, 132 (2010) 14364.
38. Z.-c. Zhang, B. Xu and X. Wang, *Chem. Soc. Rev.*, 43 (2014) 7870.
39. J. Ge, D. He, L. Bai, R. You, H. Lu, Y. Lin, C. Tan, Y.-B. Kang, B. Xiao, Y. Wu, Z. Deng, W. Huang, H. Zhang, X. Hong and Y. Li, *J. Am. Chem. Soc.*, 137 (2015) 14566.
40. T.-T. Nguyen, C.-J. Pan, J.-Y. Liu, H.-L. Chou, J. Rick, W.-N. Su and B.-J. Hwang, *J. Power Sources*, 251(2014) 393.
41. A. Roucoux, J. Schulz and H. Patin, *Chem. Rev.*, 102 (2002) 3757.
42. Y. Li, X. M. Hong, D. M. Collard and M. A. El-Sayed, *Organ. Lett.*, 2 (2000) 2385.
43. Manfred T. Reetz Prof. and E. W. Dipl.-Chem., *Angew. Chem. Int. Ed.*, 39 (2000) 165.
44. R. Franzén, *Canadian J. Chem.*, 78 (2000) 957.

45. S. U. Son, Y. Jang, J. Park, H. B. Na, H. M. Park, H. J. Yun, J. Lee and T. Hyeon, *J. Am. Chem. Soc.*, 126 (2004) 5026.
46. D. Astruc, *Inorgan. Chem.*, 46 (2007) 1884.
47. G. Berhault, L. Bisson, C. Thomazeau, C. Verdon and D. Uzio, *Appl. Catal. A*, 327 (2007) 32.
48. T. Redjala, H. Remita, G. Apostolescu, M. Mostafavi, C. Thomazeau and D. Uzio, *Oil & Gas Sci. Technol. - Rev. IFP*, 61 (2006) 789.
49. P. Tobiška, O. Hugon, A. Trouillet and H. Gagnaire, *Sensors Actuat. B- Chem.*, 74 (2001) 168.
50. T. Hübert, L. Boon-Brett, G. Black and U. Banach, *Sensors Actuat. B-Chem.*, 157 (2011) 329.
51. C. W. Xu, H. Wang, P. K. Shen and S. P. Jiang, *Adv. Mater.*, 19 (2007) 4256.
52. S.J. Hoseini, M. Bahrami, Z.S. Fard, S.F.H. Fard, M. Roushani, B.H. Agahi, R.H. Fath, S.S. Sarmoor, *Int. J. Hydrogen Energy*, 6 (2018) 1.
53. S.J. Hoseini, B.A. Habib, Z.F. Samadi, R.F. Hashemi, M. Bahrami, *Appl. Organomet. Chem.*, 31 (2017) 3607.
54. S.J. Hoseini, N. Aramesh, M. Bahrami, *Appl. Organomet. Chem.*, 31 (2017) 3675.
55. Y. Xiong, J. M. McLellan, J. Chen, Y. Yin, Z.-Y. Li and Y. Xia, *J. Am. Chem. Soc.*, 127 (2005) 17118.
56. Y. Li, G. Lu, X. Wu and G. Shi, *J. Phys. Chem. B*, 110 (2006) 24585.
57. C. Langhammer, I. Zorić, B. Kasemo and B. M. Clemens, *Nano Lett.*, 7 (2007) 3122.
58. S. Bouarab, C. Demangeat, A. Mokrani and H. Dreyssé, *Phys. Lett. A*, 151 (1990) 103.
59. D. Mendoza, F. Morales, R. Escudero and J. Walter, *J. Phys. Condens. Matt.*, 11 (1999) L317.
60. I. S. S. M. Suzuki, and J. Walter, *Phys. Rev. B*, 62 (2000) 14171.
61. S. Kishore, J. A. Nelson, J. H. Adair and P. C. Eklund, *J. Alloys Compd.*, 389 (2005) 234.
62. Y. Xiong, J. Chen, B. Wiley, Y. Xia, Y. Yin and Z.-Y. Li, *Nano Lett.*, 5 (2005) 1237.
63. Y. Xiong, B. Wiley, J. Chen, Z.-Y. Li, Y. Yin and Y. Xia, *Angew. Chem. Int. Ed.*, 44 (2005) 7913.
64. T. S. Ahmadi, Z. L. Wang, T. C. Green, A. Henglein and M. A. El-Sayed, *Science*, 272 (1996) 1924.
65. V. T. Thanh Ho, K. C. Pillai, H.-L. Chou, C.-J. Pan, J. Rick, W.-N. Su, B.-J. Hwang, J.-F. Lee, H.-S. Sheu and W.-T. Chuang, *Energ. Environ. Sci.*, 4 (2011) 4194.
66. N.R. Elezovic, V.R. Radmilovic, N.V. Krstajic, *RSC Adv.*, 6 (2016) 6788.
67. X. Sun, N. Zhang, X. Huang, *Chem. Cat. Chem.*, 8 (2016) 3436.
68. A. Kongkanand and J. M. Ziegelbauer, *J. Phys. Chem. C*, 116 (2012) 3684.
69. L.L. He, P. Song, J.J. Feng, R. Fang, D.X. Yu, J.R. Chen, *Electrochimica. Acta*, 200 (2016) 204.
70. P.K. Shen, C.W. Xu, R. Zeng, Y.L. Liu, *Electrochem. Solid-State Lett.*, 9 (2006) A39.
71. Z.L. Liu, X.H. Zhang, L. Hong, *Electrochem. Commun.*, 11 (2009) 925.
72. R.S. Amin, R.M. Abdel Hameed, K.M. El-Khatib, M. Elsayed Youssef, *Int. J. Hydrogen Energy*, 39 (2014) 2026.
73. Y. Wang, Z.M. Sheng, H.B. Yang, S.P. Jiang, C.M. Li, *Int. J. Hydrogen Energy*, 35 (2010) 10087.
74. D. Dvoranova, V. Brezova, M. Mazur, M.A. Malati, *Appl. Catal. B*, 37 (2002) 91.